Degradation of electroless Ni(P) under bump metallization (UBM) in Sn3.5Ag and Sn37Pb solders during high temperature storage

W.-M. Chen, P. McCloskey, P. Byrne, P. Cheasty, G. Duffy, J.F. Rohan, J. Boardman, A. Mulcahy, S.C. O'Mathuna

NMRC, Lee Maltings, Prospect Row, Cork, Ireland

Corresponding Author: W.-M. Chen

NMRC, Lee Maltings, Prospect Row, Cork, Ireland

wchen@nmrc.ie

Abstract:

The interfacial reaction between the electroless Ni(P) UBM and solders is studied. A P-rich layer forms in UBM along the solder side after reflow and thermal aging. Crack formation inside the P-rich layer, can sometimes penetrate throughout the entire UBM layer structure. The Ni(P) UBM degradation occurs earlier in the Sn3.5Ag solder than in Sn37Pb due to its higher reflow temperature. Despite the formation of a P-rich layer and cracks inside the UBM, it still keeps its original function within the high temperature storage period in this study. Explanations for the formation of the P-rich layer and cracks in UBM are outlined along with explanations for the Ni(P) UBM degradation process.

Key words: electronic packaging, reliability, lead free, electroless Ni(P), under bump metallization (UBM), inter-metallic compound (IMC)

1. Introduction:

Electronic packaging provides the mechanical support and electrical connection to outer circuits for devices. Improvements in silicon processing and fabrication techniques have resulted in more efficient silicon devices with significantly lower $R_{DS(on)}$ values in the region of ≤ 10 mΩ for die [1], consequently die assembly and interconnect technologies have now become the critical threshold technological barrier to achieving optimum mixed signal/ power performance [2]. To overcome these limitations, many novel packaging techniques have emerged as effective solutions in the past.

Flip chip packaging adopts direct interconnects from die to substrate through solder bumps, which differs from the conventional wire-bonding interconnection method. It offers small, light, high I/O pin counts and low profile packages, etc. thus enabling high density packaging and performance improvement of devices.

For power modules, high I/O counts are usually not required, however wire-bonding interconnections cause power loss (which contributes approximately a half of the total resistance for the power devices) and circuit speed delays [3]. Replacing wire bonds with solder bumps in power modules enables higher frequency performance, better noise control and higher power dissipation. Thus recently MOSFET manufacturers have started to provide wire-bonding-free, chip-scale packaging solutions for low voltage (20-30V) power devices in packages such as the FlipFET™ and DirectFET™ from International Rectifier, and the MOSFET-BGA from Fairchild Semiconductor.

The top metal layer of most IC bond pads is aluminium, which is suitable for conventional wire-bonding interconnection. Due to its tendency to form native oxides

quickly, the aluminium bond pad is not solderable [], an under bump metallization (UBM) transition layer is necessary for successful flip chip and solder bump interconnected power packaging.

Before UBM deposition, this native oxide should be removed through either sputtering or a chemical etching method [2, 4,5]. The UBM also acts as the barrier layer between the solder and the underlying aluminium pad protecting the fragile bondpads from fluxes and solder dissolution during reflowing, thus improving the interconnection reliability.

The UBM can be produced with a variety of techniques, such as high temperature evaporation, electroplating or electroless deposition. A wide range of materials and structures have been utilised as UBMs for flip chip packaging. Some typical UBM structures are: NiV/Cu [6]. Cr/Cr-Cu/Cu [2, 7], electroplated Ni [8], TiW/NiV [9], etc.

Recently electroless nickel has been used as UBM for flip chip packaging []. In general, acidic hypophosphite baths were used for nickel deposition, and consequently phosphorus is always incorporated in the electroless nickel deposition [10]. Through controlling the solution pH value and the deposition temperature, the phosphorus content in Ni(P) deposition can be adjusted [11]. The crystallization rate and crystallinity of Ni(P) decreases with increasing phosphorus content []. If the phosphorus content is high (>9.5 at. % [12, 13]) in the nickel plating, electroless Ni(P) will be in the amorphous state, the fast grain boundary diffusion is therefore suppressed.

Electroless Ni(P) bumping of Al bond pads followed by solder paste printing is one of the cheapest, high-volume solution routes for wafer bumping prior to flip chip assembly [].

Usually inter-metallic compounds (IMCs) will be formed between the UBM and the solder during the assembly process and device operation. If the solderable UBM layer is consumed entirely, lower adhesion or even delamination between the solder bump and substrate will be induced.

Sn/Pb based solders have been used in the electronics industry for a long time. However due to the toxic nature of Pb element, there is an increased environmental and legislative imperative to use more environmentally-friendly Pb-free alternatives. Despite the fact that no economically compatible replacements are available for Sn/Pb solders, there are many Pb free solder candidates, such as Sn3.5Ag, Sn3.5Ag0.7Cu and Sn0.7Cu, etc. Among them, the eutectic Sn3.5Ag appears to be a high strength solder with good wetting performance for most applications [14]. It has been used by some industries, such as the automotive manufacturer, Ford, and the telecommunication manufacturer, Siemens, etc.

With the continuing trend of increased integration, and the increased use of Pb-free solders in electronic packaging, it is becoming necessary to obtain an increased understanding of the reliability of lead free solders with electroless Ni(P) UBM. Actually some studies have already been done on the interfacial reaction between electroless Ni(P) UBM and liquid solders during prolonged reflow [13, 15, 16, 17, 18, 19]. In this study the interfacial reaction between eutectic Sn3.5Ag solder and electroless Ni(P) UBM is studied after one standard reflow process and different periods of high temperature storage at 150^{o}C. For comparison, the interfacial reaction between eutectic Sn37Pb solder and electroless Ni(P) UBM is also studied after the same treatments.

2. Experiments

Square solder pads with electroless Ni(P) UBM having a dimension of 800 μm x 800 μm were prepared with commercial solutions supplied by Canning UK (now McDermid UK). The process required a double zincate using a Bondal solution. The electroless nickel is deposited on the zincate treated substrates from a Nimax solution at 90^{o}C at pH 5.0. Typical deposition rates observed were 9 μm/hr. EDX analysis indicates that the P content in the electroless Ni(P) UBM is around 9.97 wt%. Our early experiments showed that a thick (>10 μm) Ni(P) UBM resulted in the UBM lifting off from the Al metallization, thus a thin (~4.5 μm) electroless Ni(P) UBM was prepared. Eutectic Sn3.5Ag and Sn37Pb solder foils with the same size were cut and put directly above the pads. Kester RMA rosin flux was used during reflow for higher quality solder bumps. Reflow was achieved in a programmable SRO-702 IR oven under N_2 atmosphere according to the recommended profiles from solder manufacturers. The peak reflow temperatures used for eutectic Sn37Pb (MP: 183^{o}C) and Sn3.5Ag (MP: 221^{o}C) solders are 210^{o}C and 250^{o}C respectively. The achieved height for the solder bumps was approximately 300 μm.

High temperature storage was performed in a Heraeus VöTSCH oven at (150^{o}C ± 1^{o}C). Samples were removed from oven for cross-section microstructure analysis after reaching the designed storage time. For each high temperature storage time at 150^{o}C and solder composition, a different symbol was assigned (Table 1).

Two solder bumps were chosen for cross sectional analysis. This process involved mounting the samples in epoxy, the cured assemblies were then ground in a Metaserv 2000 grinder with different grade SiC papers sequentially, and finally polished with 1 μm and 0.5

μm Al_2O_3 suspensions respectively. A Leitz Nomarski microscope was used to check the cross-sectioned samples to observe the UBM morphology following the different periods of high temperature exposure. The cross-sectioned samples were also analysed using a Hitachi S-4000 scanning electron microscope (SEM). The average thickness of the different compositional layers within the cross-sectioned samples were measured by the SEM. An attached Princeton Gamma-Tech energy dispersive X-ray (EDX) spectroscopy analysis system was used for elemental analysis. Before SEM analysis, the cross-sectioned samples were etched in acid solutions for a few seconds to improve the image contrast, then coated with a thin gold layer to assist the measurements.

3. Results and analysis

3.1 Effects of reflow and thermal aging on Ni(P) UBM microstructure in Sn3.5Ag solder

Both the Nomarski and SEM images of Sn3.5Ag cross-sectioned samples indicated that the UBM morphology changed during solder bump thermal aging at 150^{o}C. A few typical cross-sectioned Nomarski or SEM images are shown in Fig. 1.

Immediately after solder bump reflow (sample Free0), the Ni(P) UBM is composed of two parts. EDX analysis shows that the layer neighbouring the solder has a higher P content of around 14.79wt%, which is very close to the composition of Ni_3P. It indicates that this layer is composed of polycrystalline Ni_3P [], which is caused by the self-crystallization of amorphous Ni(P) during reflow and the solder reaction-assisted crystallization of electroless Ni(P) UBM [[13,19]]. Usually the self-crystallization of amorphous Ni(P) occurs only above

250^{o}C and after hours of annealing []. In contrast, the layer between the P-rich layer and Al metallization has a lower P content of around 10.15wt%, which is very close to the original P content in the electroless Ni(P) UBM, 9.97wt%. In this paper, this layer is referred as the original Ni(P) layer. After thermal aging, the thickness of P-rich layer increases, while the original Ni(P) layer thickness decreases. Meanwhile cracks start to appear in the P rich layer (Figs. 1b, 1c), while some cracks even penetrate into the original Ni(P) layer (as indicated inside the dotted squares in Fig.1b). Such cracks were also reported in the Ni(P) UBM after prolonged reflow at 240^{o}C [].

Under high temperature at reflow or thermal aging at 150^{o}C, Ni atoms from Ni(P) UBM will react with Sn atoms from the solder to form Ni-Sn IMCs []. With the diffusion of Ni atoms into solder and Ni-Sn IMCs formation, P content increases at the solder side of Ni(P) UBM, thus a P-rich layer formed in the Ni(P) at the solder side. Actually P atoms also diffuse into the solder, as the P concentration in Ni(P) UBM is higher than in the solder, which is evidenced by the elemental X-ray map shown in Fig. 2, which is taken after 1500 hours thermal aging, i.e. sample Free4. This is in contrast to one report that P did not diffuse into the solder []. Fig. 2 shows that P distributes all over the solder bump while some P elements even diffuse into the Si side of the chip. Hence the formation of P-rich layer in Ni(P) UBM is caused by the different diffusion rate between P and Ni. Ni atoms diffuse more quickly than P and this may be caused by the fact that Ni-Sn IMCs formation occurs soon after Ni atoms reach the solder. Consequently most Ni atoms exist in the Ni-Sn IMCs in a combined state (see Fig. 2); while most P atoms are in the free state (which will be explained later), thus the free Ni atom concentration in the solder is lower than that of P, and hence the driving force for Ni diffusion is higher. A P-rich layer therefore forms in Ni(P) UBM at the solder side.

In our cross-sectioned samples, EDX measurements indicate that the P content in the original Ni(P) layer keeps increasing with duration of thermal aging, which differs substantially from results reported in literature []. Some EDX elemental analysis results are listed in Table 2, while the calculated stoichiometric compositions of the corresponding spots are listed in Table 2. The increase of P content in the original Ni(P) layer is caused by the Ni concentration gradient inside the Ni(P) UBM. After more Ni atoms have diffused into the solder, more of the original Ni(P) regions turn into new P-rich regions. So the original Ni(P) layer thickness keeps decreasing while the P-rich layer keeps growing. Finally, the original Ni(P) layer disappears completely in Sn3.5Ag solder after aging at 150^{o}C for 1500 hours (Fig. 1c).

During reflow or thermal aging, the loss of Ni atoms from Ni(P) UBM is unlikely to be uniform across the whole Ni(P) UBM. As a result, the P-rich layer thickness is not uniform across the Ni(P) UBM (refer to Fig. 1b). In some regions, atoms may diffuse faster and small voids will form in the Ni(P) UBM, finally as void size increases, cracks start to appear in Ni(P) UBM. As more atoms diffuse away from the P-rich layer, more cracks are formed in the P-rich layer. Increased thermal aging significantly increases crack formation in the Ni(P) UBM (see Fig. 1c).

Direct evidence that Ni atoms diffuse also from the original Ni(P) layer into the solder is presented by the formation of cracks which penetrate into the original Ni(P) layer (Fig. 1b).

The Ni-P compounds in the P-rich layer were found to have the following forms: Ni_3P, Ni_2P, Ni_5P_4 and NiP_2 []. The 16.1wt% P content inside the cracks indicates that the initially-formed Ni_3P continues to lose Ni, thus some higher P content Ni-P compounds, like Ni_2P, Ni_5P_4, etc. may have already formed around these cracks.

In addition, EDX analysis shows the presence of small amounts of Sn in the Ni(P) UBM for sample Free1 and other samples exposed to longer periods of thermal aging. The Sn content is higher in the P-rich layer, and even higher inside the cracks (refer to Table 2). Diffusion of Sn atoms into the Ni(P) UBM indicates the start of degradation of the Ni(P) UBM. However, the Sn content in the UBM of our samples is still much lower than that (~15.0 wt% or 7.3 at%) in the P-rich layer of Ni(P) UBM after 1 minute reflow at 250^{o}C reported in the literature []. Longer periods of thermal aging may induce higher Sn content in the P-rich layer and final Ni(P) UBM failure.

Despite the formation of a P-rich layer and Sn diffusion into the Ni(P) UBM, both cross-sectioned Nomarski and SEM images indicated that the P-rich layer did not lift off from the Sn3.5Ag solder or the underlying Al even when there was no original Ni(P) layer left in the UBM after 1500 hours aging at 150^{o}C. The solder bump shear strength did not show an obvious decrease either (this will be reported elsewhere). These results mean that the P-rich layer can still function as a UBM, but cracks and Sn diffusion in the P-rich layer indicate that P-rich layer is not as effective as the original Ni(P) layer as a UBM.

The total Ni(P) UBM thickness (which includes the original Ni(P) layer plus the P-rich layer) at different stages is presented in Fig. 3. This shows clearly that the total thickness continues to decrease during thermal aging. But the rate of decrease differs at the early (0 to 500 hours) and late stages (500 to 1500 hours). During the early thermal aging period, the UBM is consumed quickly, while it is consumed at a slower rate in the later stages. Unlike the early thermal aging, after 500 hours, the major part of the UBM has transferred into the P-rich layer, the results in Fig. 3 show that the P-rich layer has a slower reaction rate with the Sn3.5Ag solder. This may be caused by the longer Ni diffusion

distance and lower Ni content in the P-rich layer in the later stages, thus a lower IMCs formation rate results.

In addition to the Ni(P) UBM, the IMCs were also checked in the cross-sectioned samples. Both optical and electron microscopy confirm that IMCs form after solder reflow and thermal aging. However no continuous Ni-Sn IMCs layer was observed after reflow or after different periods of thermal aging. Instead chunky or needle-like Ni-Sn IMCs were detected along the interface or inside the solder body, i.e. parts of the IMCs in Ni(P)/SnAg solder interface were observed to be detaching from the interface and moving towards the solder body. Similar results were reported in the literature during prolonged reflow processes, e.g. 30 minutes for similar sample systems []. However, along bump edges more Ni-Sn IMCs are found at the interface. This may be caused by the fact that there is less solder surrounding the interface along edges, thus the IMCs detaching from the interface is restricted around solder bump edges, as a result, more IMCs adhere to the interface.

EDX analysis results show that these IMCs are composed of Ni and Sn. The stoichiometric composition of the interface Ni-Sn IMC in sample Free2 is $NiSn_{0.91}$, no P is detected in the EDX spectrum of IMCs. This implies that P tends to be expelled from the Ni-Sn IMC crystal structures. Most P atoms are in a free state as compared to the Ni atoms in the solder. However P was reported to be entrapped in the Ni-Sn IMCs for SnAg solder due to the rapid reaction of electroless Ni(P) with SnAg solder [].

There are three kinds of Ni-Sn IMCs, Ni_3Sn_4, Ni_3Sn_2 and Ni_3Sn though [], usually only Ni_3Sn_4 is reported in the literature [[13,16]]. As Ni_3Sn_4 is thermodynamically the most stable one among all Ni-Sn IMCs [], it is usually the first formed IMC after short interface reaction. The IMCs existing inside Free2 are obviously not pure Ni_3Sn_4, the long thermal aging (500 hours) may have caused Ni_3Sn_4 partially transfer into the lower Sn content Ni-

Sn IMCs, Ni_3Sn_2 or even Ni_3Sn. This implies that the Ni-Sn IMCs are formed at the solder side, Ni atoms are the diffusion species. From the stoichiometric composition of the Ni-Sn IMC in Free2, it can be seen that this transformation is not complete at this stage, i.e., part of the IMCs are still in the form of Ni_3Sn_4.

3.2 Effects of reflow and thermal aging on Ni(P) UBM microstructure in Sn37Pb solder

For Sn37Pb solder, a double layer of UBM is also observed with optical Nomarski and SEM microscopy after different periods of thermal aging, however this double layer is not observed for solder bumps immediately after the standard reflow at 210^{o}C. Moreover the P-rich layer is thinner as compared to that of Sn3.5Ag solder bumps under the same treatment. Two typical cross-sectioned images at different stages are shown in Fig. 4. After 1500 hours thermal aging at 150^{o}C, only about half of the Ni(P) UBM thickness has turned into the P-rich layer. Similarly a few cracks start to appear in the P-rich layer or even the whole Ni(P) UBM after long periods of thermal aging, however no Sn atoms are detected in either layer. These results show that Ni(P) UBM is more reliable if used with Sn37Pb solder.

Unlike the case of Sn3.5Ag solder, a dense and continuous Ni-Sn IMCs is found along Ni(P)/Sn37Pb solder interface after reflow and different periods of thermal aging (see Figs. 4a, 4b). EDX analysis indicates that the stoichiometric IMCs composition is around $NiSn_{0.86}$ with small variations at different regions for sample Lead4. Compared with the IMC composition of sample Free2, it is found that the Sn content in Lead4 is lower. Lead4 undergoes longer thermal aging than Free2, the result here confirms our previous

assumption that the Ni-Sn IMCs are transferring gradually from Ni_3Sn_4 into the lower Sn content Ni-Sn IMCs, Ni_3Sn_2 and Ni_3Sn, during thermal aging.

The good linear relation between the average IMCs thickness and the square root of thermal aging time (Fig. 5) implies that the IMCs formation is a diffusion controlled process [20].

3.3 Comparison of the effects of thermal aging on the P-rich layer thickness in Ni(P) UBM between Sn3.5Ag and Sn37Pb solders

As indicated previously, a P-rich layer appears in the Ni(P) UBM for both solders, a thinner P-rich layer is formed in the Sn37Pb solder. The higher Sn content and higher reflow temperature of eutectic Sn3.5Ag solder are regarded as the reasons for this difference []. Relations between the average P-rich layer thickness after different periods of thermal aging at 150^{o}C for both solders and the square root of aging time are shown in Fig. 6. It shows that the P-rich layer formation is also characteristic of a diffusion controlled process, but the formation rate is different at different thermal aging stages. At the early (0 to 500 hours) stage, the P-rich layer thickness increases quickly, but it increases a little more slowly at the late (500 to 1500 hours) stages of thermal aging. Fig. 3 shows that the total Ni(P) UBM thickness in Sn3.5Ag solder keeps decreasing. After 1500 hours, the original Ni(P) UBM disappears completely. It is expected that the P-rich layer thickness in Sn3.5Ag solder will start to decrease after 1500 hours and this P-rich layer will eventually disappear as a result of IMC formation. In the literature, it is reported that under the reflow temperature of 240^{o}C, the original Ni(P) UBM disappeared after 30 minutes, and the whole

Ni(P) layer disappeared after 180 minutes in the case of a Ni(P) UBM with an initial thickness of 3 μm [].

An interesting feature of Fig. 6 is that the P-rich layer formation rate during thermal aging at 150^{o}C does not show a significant difference between Sn37Pb and Sn3.5Ag solders except that the initial P-rich layer formed during higher temperature reflow for Sn3.5Ag solder. This finding differs from the reports in literature []. Despite the higher Sn content in Sn3.5Ag solder, it does not accelerate the rate of P-rich layer formation under the same thermal aging conditions. As the concentration of free Sn atoms reacting with Ni atoms from Ni(P) UBM in Sn37Pb solder is sufficiently high, and the P-rich layer formation is a diffusion controlled process, the Sn content in solder does not affect the P-rich layer formation.

3.4 Ni(P) UBM degradation process

Based on the knowledge obtained from this study and the literature, it is reasonable to conclude that the Ni(P) UBM degradation includes the following steps:

1) Formation of P-rich layer, which is composed of crystalline Ni_3P at the beginning. For Sn3.5Ag solder, this starts during solder bump reflow and continues throughout the thermal aging process. For Sn37Pb solder, this happens mainly during the solder bump thermal aging process after reflow.

2) Ni atoms continue diffusing from the P-rich layer and the original Ni(P) layer to the UBM/solder interface where Ni-Sn IMCs are formed, thus the P-rich layer thickness keeps increasing and the original Ni(P) layer thickness keeps decreasing.

3) Cracks develop in the P-rich layer, some cracks penetrate to the original Ni(P) UBM layer.

4) Sn starts to diffuse into the Ni(P) UBM. Around the cracks, the Sn content is higher.

5) The original Ni(P) layer diminishes until only a P-rich layer is left between the solder and the aluminium pad.

6) Ni atoms continually diffuse from the P-rich layer and higher P content Ni-P compounds, such as Ni_2P and Ni_5P_4, or even higher P content Ni-P compound NiP_2 start to appear in the P-rich layer. Meanwhile the P-rich layer thickness keeps decreasing. This process continues until all the Ni(P) UBM disappears. After that, delamination of solder bumps will occur, solder bumps lose adhesion to the underlying pad, and the solder bump interconnection fails completely.

Each of the steps in the mechanism described here is not necessary discrete. It is evident that several of the individual processes can progress concurrently.

4. Conclusion

During reflow or thermal aging, Ni atoms in electroless Ni(P) UBM diffuse to the UBM/solder interface to form Ni-Sn IMCs. A P-rich layer forms in UBM at the solder side as a result of diffusion rate differences between Ni and P. During aging the total Ni(P) UBM thickness decreases, but at different rates at different stages - it is consumed quickly at the beginning, and more slowly at the late stage. It was found that the Ni(P) UBM

degrades earlier with Sn3.5Ag solder than in Sn37Pb solder. Electroless Ni(P) UBM is more reliable when used for the Sn37Pb solder than for the Sn3.5Ag solder.

Formation of the P-rich layer is a diffusion controlled process, its thickness keeps increasing within our thermal aging periods. It occurs quickly at the beginning and more slowly at later stages, while the original Ni(P) layer thickness decreases. The rate of P-rich layer thickness increase is not affected by the solder types during high temperature storage. In Sn3.5Ag solder, the original Ni(P) UBM disappears after long period of thermal aging at 150^{o}C. Cracks form inside the P-rich layer, sometimes these cracks penetrate the whole UBM layer. Sn atoms start to diffuse into the Ni(P) UBM after crack formation. Around cracks, the Sn content is higher.

A continuous Ni-Sn IMCs layer forms at the UBM/solder interface by diffusion controlled process for Sn37Pb solder while no similar continuous IMCs layer is observed for Sn3.5Ag solder, instead some IMCs in Sn3.5Ag drift towards the solder bulk. IMCs in the interface change from Ni_3Sn_4 into Ni_3Sn_2 and Ni_3Sn during thermal aging.

Acknowledgment: W.-M. Chen is indebted to Dr. K. Thomas and J. Pike for allowing use of Nomarski microscope.

Table captions

Table 1 High temperature storage time and sample symbols.

Table 2 EDX Elemental analysis results on different regions of Ni(P) UBM

Table 1

High temperature storage time (Hours)		0	200	500	1000	1500
Solder type	Sn3.5Ag	Free0	Free1	Free2	Free3	Free4
	Sn37Pb	Lead0	Lead1	Lead2	Lead3	Lead4

Table 2

Sample No.	In double layers		Inside cracks	In P-rich layer: away from cracks
	The original Ni(P) layer	P-rich layer		
Free0	Ni 89.85wt% P 10.15wt% $Ni_{0.824}P_{0.176}$	Ni 85.21wt% P 14.79wt% $Ni_{0.753}P_{0.247}$		
Free1	Ni 88.75wt% P 11.08wt% Sn 0.18wt% $Ni_{0.808}P_{0.191}Sn_{0.001}$	Ni 84.71wt% P 14.53wt% Sn 0.76wt% $Ni_{0.753}P_{0.244}Sn_{0.003}$		
Free4			Ni 82.89wt% P 16.10wt% Sn 1.01wt% $Ni_{0.728}P_{0.268}Sn_{0.004}$	Ni 83.52wt% P 15.87wt% Sn 0.61wt% $Ni_{0.733}P_{0.264}Sn_{0.003}$

Figure captions

Figure 1 Nomarski or SEM images of cross-sectioned lead free samples (a) immediately after one standard reflow (SEM image), Free0; (b) after 200 hours (Nomaski image), Free1. a SEM crack image in the P-rich layer is shown as inset; (c) after 1500 hours (Nomarski image), Free4, thermal aging at 150^{o}C.

Figure 2 X-ray mapping for elemental distribution from the cross-sectioned Free4 sample.

Figure 3 Ni(P) UBM thickness decrease with Sn3.5Ag solder during high temperature storage @ 150^{o}C.

Figure 4 Typical cross-sectioned images of Sn37Pb solder samples (a) immediately after one standard reflow (Nomaski image), Lead0; (b) after 1500 hours (SEM image), Lead4, thermal aging at 150^{o}C.

Figure 5 IMCs thickness increase for Ni(P)/Sn37Pb solder with high temperature storage @ 150^{o}C.

Figure 6 P rich layer thickness increase during high temperature storage @ 150^{o}C.

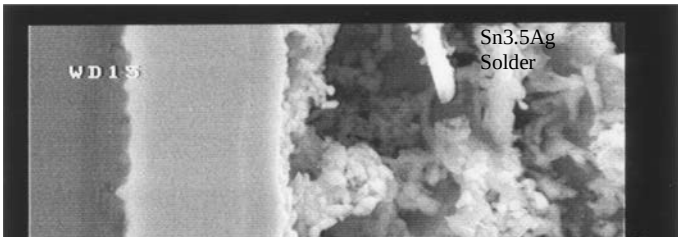

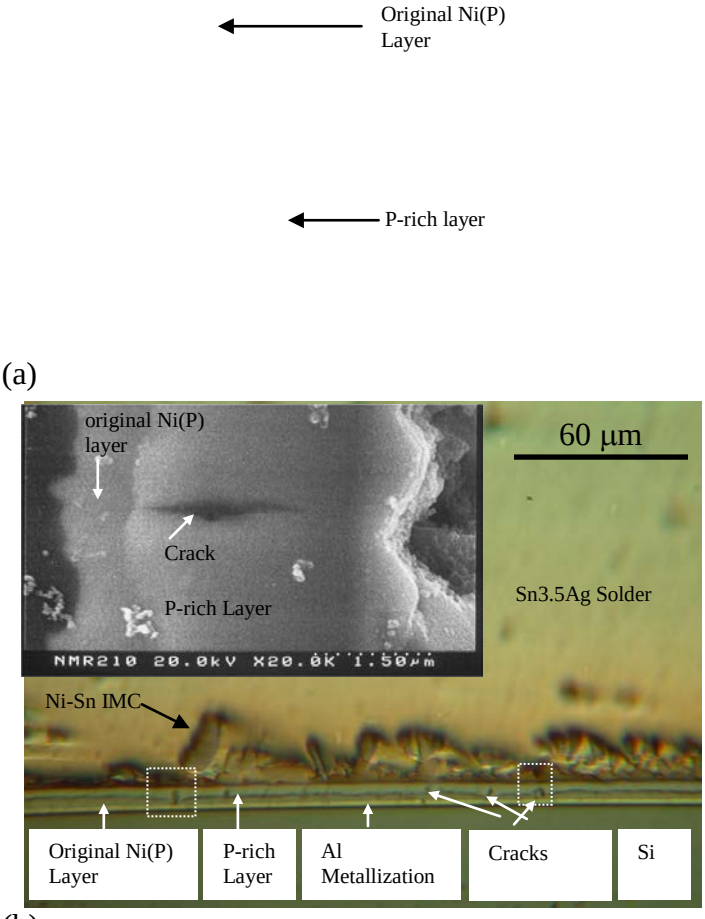
Original Ni(P)
Layer
P-rich layer
(a)
original Ni(P)
layer
Crack
P-rich Layer
NMR210 20.0kV X20.0K 1.50µm
60 µm
Sn3.5Ag Solder
Ni-Sn IMC
Original Ni(P)
Layer
P-rich
Layer
Al
Metallization
Cracks
Si
(b)
60 µm
Ni-Sn IMCs
P-rich Layer
Cracks
(c)

Figure 1

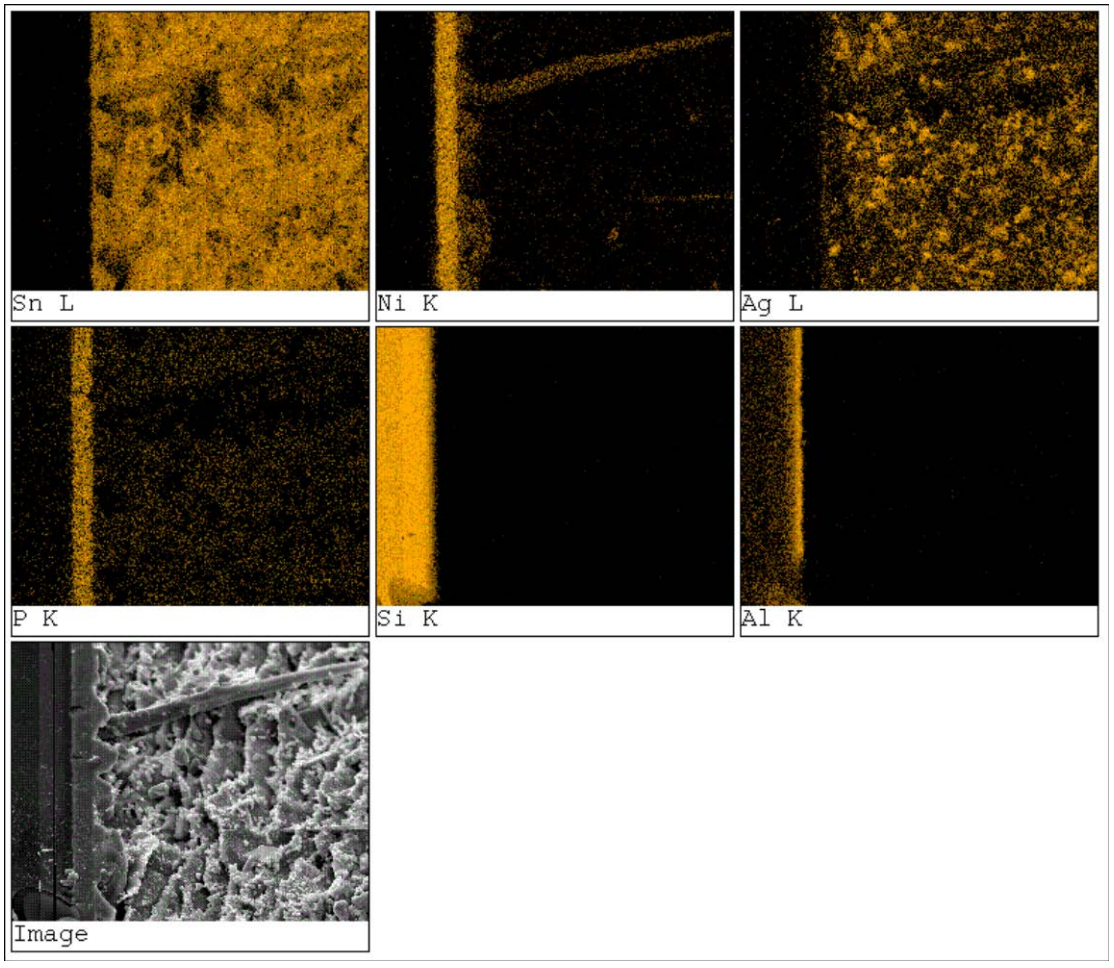

Figure 2

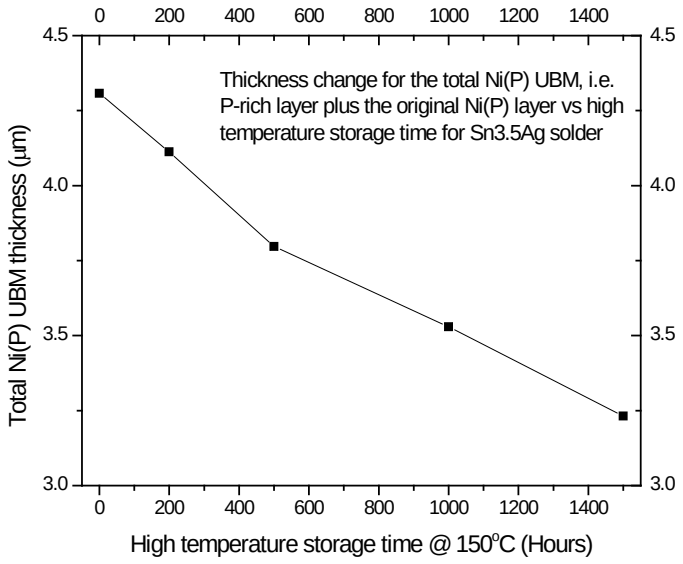
Thickness change for the total Ni(P) UBM, i.e. P-rich layer plus the original Ni(P) layer vs high temperature storage time for Sn3.5Ag solder
Total Ni(P) UBM thickness (μm)
High temperature storage time @ 150°C (Hours)
0
200
400
600
800
1000
1200
1400
4.5
4.0
3.5
3.0

Figure 3

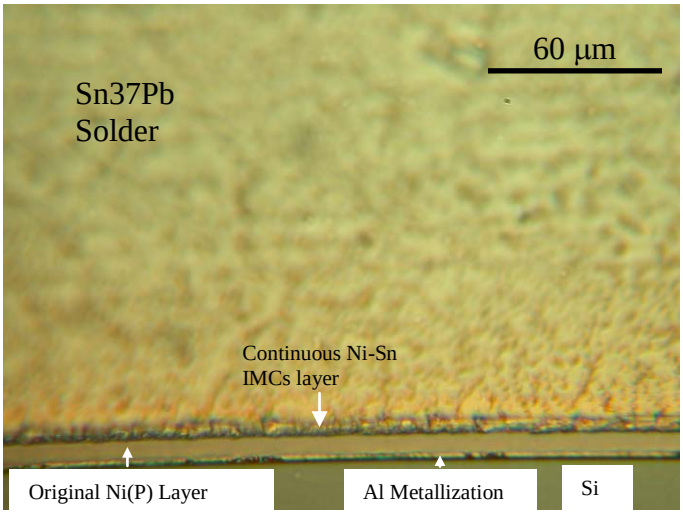
60 μm
Sn37Pb
Solder
Continuous Ni-Sn
IMCs layer
Original Ni(P) Layer
Al Metallization
Si

(a)

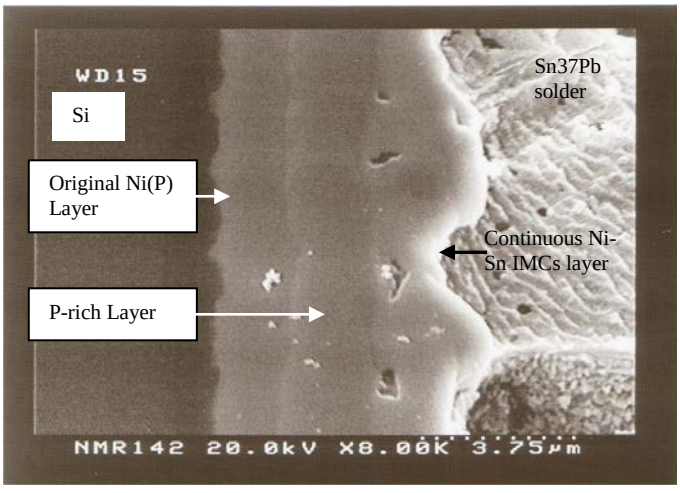
WD15
Si
Original Ni(P)
Layer
P-rich Layer
Sn37Pb
solder
Continuous Ni-
Sn IMCs layer
NMR142 20.0kV X8.00K 3.75μm

(b)

Figure 4

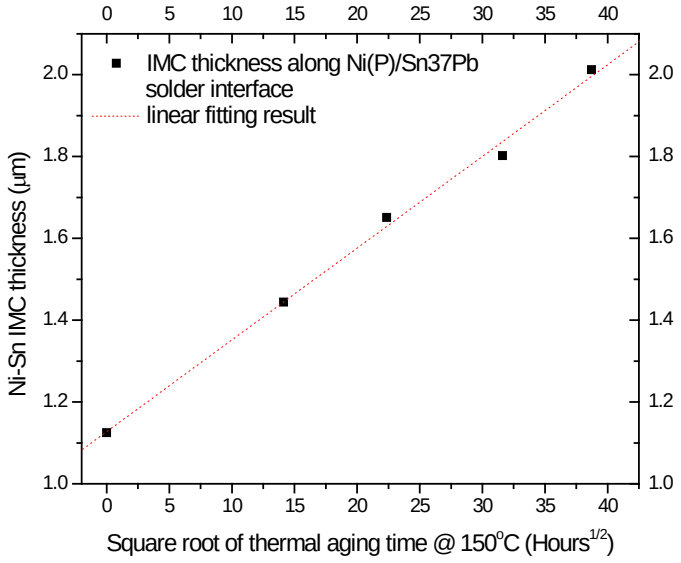
IMC thickness along Ni(P)/Sn37Pb solder interface
linear fitting result
Ni-Sn IMC thickness (μm)
Square root of thermal aging time @ 150°C (Hours^1/2)
0
5
10
15
20
25
30
35
40
1.0
1.2
1.4
1.6
1.8
2.0

Figure 5

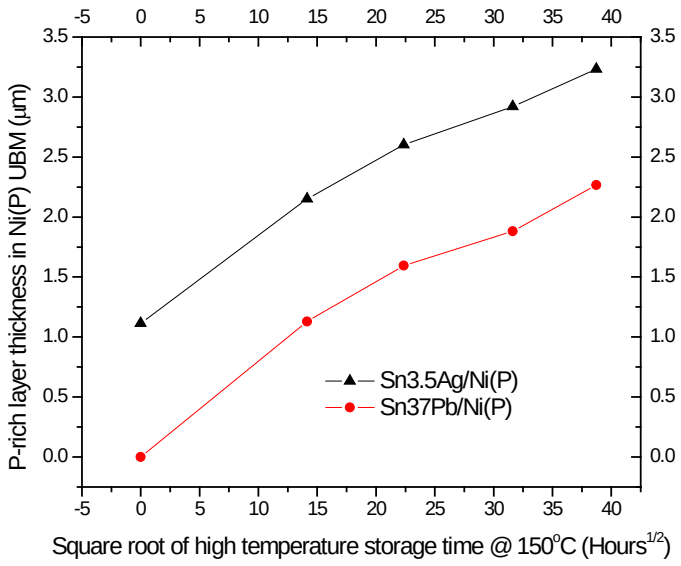

Figure 6

5. Reference

[1] A. Tsui, M. Kasem, W. McDaniel, E. Lambka, PCIM Power Electronic systems, 25, 20 (1999).

[2] R.R. Tummala, E.J. Rymaszewski, Microelectronics Packaging Handbook, (1989), Van Nostrand Reinhold.

[3] S.C. O'Mathuna, P. Byrne, G. Duffy, W. Chen, M. Ludwig, T. O'Donnell, P. McCloskey, IECON Proceedings (Industrial Electronics Conference, SEVILLA, Spain), 4, 3250 (2002).

[4] R. Aschenbrenner, A. Ostmann, U. Beutler, J. Simon, H. Reichl, IEEE Trans. Comp. Packag. Technol., Part B, 18, 334 (1995).

[5] D.A. Hutt, C. Liu, P.P. Conway, D.C. Whalley, S.H. Mannan, IEEE Trans. Comp. Packag. Technol., 25, 87 (2002).

[6] F. Zhang, M. Li, B. Balakrisnan, W.T. Chen, TMS; IEEE. J. Electron. Mater., 31, 1256 (2002).

[7] K.S. Kim, C.H. Yu, N.H. Kim, N.K. Kim, H.J. Chang, E.G. Chang, Microelectron Reliab, 43, 757 (2003), and reference therein.

[8] S.M. Chang, R.H. Uang, D.C. Liou, H.T. Hu, K.C. Chen, Y.F. Chen, Y.H. Chen, ECTC2003, 1209-1214.

[9] S.Y. Jang, K.W. Paik, Advances in Electronic Materials and Packaging 2001 (Piscataway, NJ, USA.), 2001, pp.121-8.

[10] D.A. Hutt, C. Liu, P.P. Conway, D.C. Whalley, S.H. Mannan., IEEE Trans. Comp. Packag. Technol., 25, 98 (2002).

[11] J.F. Rohan, G. O'Riordan, Microelectron. Eng., 65, 77 (2003).

[12] M.O. Alam, Y.C. Chan, K.C. Hung, Microelectron Reliab., 42, 1065 (2002), and reference therein.

[13] J.W. Jang, P.G. Kim, K.N. Tu, D.R. Frear, P. Thompson, J. Appl. Phys., 85, 8456 (1999), and reference therein.

[14] http://www.boulder.nist.gov/div853/lead%20free/part1.html# 1.19.

[15] C. Y. Lee, K.L. Lin, Thin solid films, 249, 201 (1994), and reference therein.

[16] Y.D. Jeon, K.W. Paik, ECTC2001, and reference therein.

[17] K.C. Hung, Y.C. Chan, C.W. Tang, H.C. Ong, J. Mater. Res., 15, 2534 (2000).

[18] M.O. Alam, Y.C. Chan, K.C. Hung, J. Electron. Mater. 31, 1117 (2002).

[19] K. Zeng, K.N. Tu, Mater. Sci. Eng. Rep. 38, 55 (2002).

[20] G. M. Barrow, Physical Chemistry, (1961), London, McGRAM-HILL Book Company, Inc.